ChemComm

Accepted Manuscript

This article can be cited before page numbers have been issued, to do this please use: A. Maignan, C. Martin, O. I. Lebedev, J. Sottmann, L. Nataf, F. Baudelet, S. Hébert and R. carbonio, *Chem. Commun.*, 2019, DOI: 10.1039/C9CC00926D.

ROYAL SOCIETY OF CHEMISTRY

rsc.li/chemcomm

View Article Online
DOI: 10.1039/C9CC00926D

COMMUNICATION

$Sr_2Fe_{1+x}Re_{1-x}O_6$ double perovskite: magnetoresistance and (magneto)thermopower

Received 00th January 20xx,
Accepted 00th January 20xx

DOI: 10.1039/x0xx00000x

Antoine Maignan[1], Christine Martin[1], Oleg Lebedev[1], Jonas Sottmann[1], Lucie Nataf[2], François Baudelet[2], Sylvie Hébert[1] and Raúl E. Carbonio[3]

Polycrystalline $Sr_2Fe_{1+x}Re_{1-x}O_6$ samples have been synthesized and structurally characterized by X-ray powder diffraction, transmission electron microscopy and X-ray absorption spectroscopy. Resistivity strongly increases with x, but a large and negative magnetoresistance persists up to x = 0.33. This is discussed considering the charge delocalization in iron and rhenium t_{2g} orbitals.

Among the thermoelectric oxides, the n-type members usually contain d^0 or d^{10} cations such as $Sr_{1-x}La_xTiO_3$ [1], TiO_2 [2] or also overdoped In_2O_3 [3] and ZnO [4]. These compounds containing magnetic cations with partially filled *3d* or *4d* orbitals are scarce, being almost limited to perovskites such as n-type manganites, derived from $CaMnO_3$ [5] or double perovskites such as Sr_2FeMoO_6 [6]. For their p-type counterparts, large Seebeck (S) values are usually related to a spin and orbital entropy term that increases S at high temperature as shown for layered cobaltites like $Ca_3Co_4O_9$ [7], $SrRuO_3$ and related [8] or p-type manganites [9].

The magnetic cations can have another beneficial effect, as the magnetic entropy associated to paramagnetic spins can enhance the Seebeck coefficient in the low temperature as well, as the magnetic susceptibility increases, as in Na_xCoO_2 [10], $Ca_3Co_4O_9$ [11] or $CuCrTiS_4$ [12]. This extra term can be evidenced by magnetothermopower (MTEP) experiments. However, to the best of our knowledge such MTEP experiments have not been reported yet for n-type ferrimagnetic oxides. Looking for candidates, it turns out that ordered magnetic double perovskites would be appropriate as their magnetic ordering temperature can be beyond room temperature as in A_2FeMO_6 (A=Ca, Sr, Ba; M=Mo, Re) showing room temperature (RT) magnetoresistance [13, 14]. Furthermore, this coupling between spins and charges appears to be an advantage to search for MTEP effects if one refers to the p-type oxides [10, 11].

Among the double perovskites, ferrimagnetic $Sr_3Fe_2ReO_9$ attracted our attention [15]. Indeed, as this compound crystallizes in the *I*4/*m* space group, with *a*≈5.67Å and *c*≈7.90Å, that is characteristic of Ae_2FeMO_6 double perovskites, its formula must be written as $Sr_2Fe_{4/3}Re_{2/3}O_6$ [16]. In the $Sr_2Fe_{1+x}Re_{1-x}O_6$ series, the degree of cationic ordering (the distribution of Fe and Re on 2*a* and 2*b* Wyckoff sites) has an effect on the magnetic properties, whatever x [17-20].

We report on the synthesis, structural characterization by X-ray powder diffraction (XRPD) and transmission electron microscopy (TEM) of polycrystalline samples of the $Sr_2Fe_{1+x}Re_{1-x}O_6$ series. Magnetic and (magneto)resistance (MR) measurements were performed, and MTEP measurements for $Sr_2Fe_{1.33}Re_{0.67}O_6$, corresponding to x = 0.33 and reported to be single phase [15], to investigate the transport mechanism and its relationship to a 'double-exchange' like mechanism.

SrO, Fe_2O_3, ReO_3 and Re precursors were weighed (to obtain about 1g of mixture) according to the stoichiometric $Sr_2Fe_{1+x}Re_{1-x}O_6$ formula, with x = 0, 0.25, 0.33, 0.375, 0.5 and 0.75. After crushing and mixing, the powders were pressed in bars (2x2x10mm), which were set in alumina crucibles themselves inserted in silica tubes. After sealing (under primary vacuum ≈1 mbar), the tubes were heated at 1200°C in 12hr, left at this temperature for 24hr, and then cooled down to RT in 12hr. The structural properties were checked by RT XRPD with a PAN-analytical diffractometer (CoK_α radiations). The crystallographic structures were refined in the *I*4/*m* space group of the double perovskite $Ae_2MM'O_6$ structure [16] using the Fullprof program
[21]. Since scattering factors for Re and Fe are quite different, occupation of the metal 2*a* and 2*b* Wyckoff sites were refined. The local cation ordering was studied at the atomic scale using a HAADF-STEM ARM 200F cold FEG. Three $Sr_2Fe_{1+x}Re_{1-x}O_6$ samples with x= 0, 0.25 and 0.33 were characterized by X-ray absorption near structure (XANES) at ODE beamline at SOLEIL synchrotron (Saclay, France). The Fe K-edge X-ray absorption spectra were measured in a transmission configuration using a bent crystal as polychromator, with a focal area of 25 × 25 μm^2 at full width at half-maximum, and with an energy resolution of 0.5 eV. The spectra were acquired with a position-sensitive detector and calibrated in energy using an iron metal foil. For the measurement, finely ground samples and references were loaded in diamond anvil cells and mounted in the focal point of

[1] *Laboratoire CRISMAT, UMR 6508 CNRS/ENSICAEN/UCBN, 6 bd du Maréchal Juin, 14050CAEN Cedex 4, France*
[2] *Synchrotron Soleil, Saint-Aubin BP 48, 91192 GIF-SUR-YVETTE CEDEX, France*
[3] *INFIQC (Consejo Nacional de Investigaciones Científicas y Técnicas [CONICET]– Universidad Nacional de Córdoba), Departamento de Fisicoquímica, Facultad de Ciencias Químicas, Universidad Nacional de Córdoba, Haya de la Torre Esq. Medina Allende, Ciudad Universitaria, X5000HUA Córdoba, Argentina Address here.*

Electronic Supplementary Information (ESI) available: [details of any supplementary information available should be included here]. See DOI: 10.1039/x0xx00000x

the X-ray beam. FeO and Fe_2O_3 were used as reference materials for the Fe K-edge spectra that were collected in the 7090–7240 eV. The XANES spectra were normalised using ATHENA [22]. The magnetic properties were studied using a

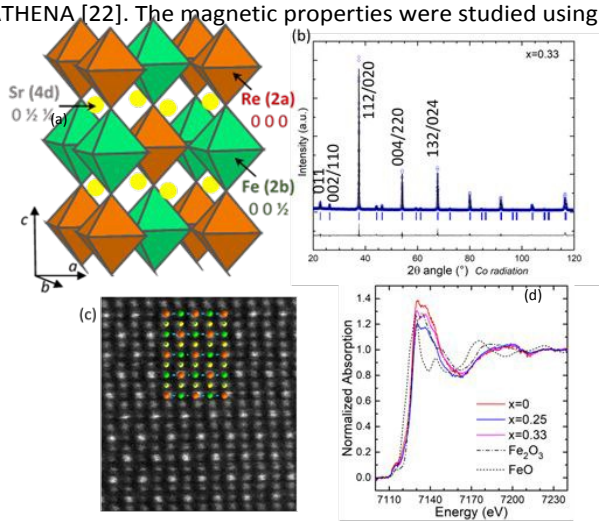

Figure 1: (a) Drawing of the perfectly ordered structure of Sr_2FeReO_6 (x = 0). (b) RT XRPD patterns (observed, calculated and difference plots and Bragg ticks) of the x=0.33 sample. (c)[100] HAADF TEM image of x=0.33 with the superimposed structural model (code colour is same as for (a): Sr, yellow; Fe, green; Re, orange; O, blue). (d) Normalized Fe K-edge absorption spectra of $Sr_2Fe_{1+x}Re_{1-x}O_6$ (x = 0, 0.25 and 0.33) compared to Fe_2O_3 (Fe^{3+}) and FeO (Fe^{2+}) as references.

SQUID magnetometer (5T-MPMS, Quantum Design). Electrical contacts were made on bars using silver paste and a physical property measurement system (9T-PPMS, Quantum Design) was used for the four probe resistivity (ρ) measurements. A home-made steady-state technique was used to measure the TEP and MTEP in the 9T-PPMS. For T>300K, a ULVAC ZEM3 system was also used to measure S.

The XRPD patterns are all characteristic of the I4/m double perovskite except for x=0.75, which crystallizes as a cubic $Pm\bar{3}m$ perovskite ($SrFe_{0.625}Re_{0.375}O_3$). For all other samples (x≤0.5), refinements were performed to obtain cell parameters and occupancies of both 2*b* and 2*a* Fe/Re sites (Fig.1a). These results are summarized in Table 1 showing a good agreement between the calculated and nominal compositions and a very small evolution of cell parameters versus x. The composition values should be taken with caution since a few impurities are sometimes observed (at low level), as the oxygen stoichiometry is supposed to be 6 whatever x, but in most of the cases, the refined values are very close to the nominal ones. The x=0 composition corresponds to a "perfect" order due to the ideal Fe/Re=1 ratio and the occupation of each site by only one cation (Fe on 2b and Re on 2a). Up to x = 0.5, as x increases, refinements indicate different occupations of the 2b and 2a sites, the 2b mainly occupied by Fe, while the 2a site Re content decreases (Table 1). It shows that a preferential occupation is preserved below x = 0.5. Finally, the x=0.75 sample is a single perovskite. Nevertheless the Sr_2FeReO_6 ordered double perovskite is difficult to prepare. For instance, high pressure is required [17] or a Re excess is needed at normal pressure [18-20]. In normal synthesis condition, the x=0 compound tends to form anti-site defects detrimental to the ferrimagnetic ordering, leading thus to a reduced saturation magnetization (M_s) and to a T_C increase [18-20]. In our synthesis conditions, as an impurity is observed in the XRPD pattern of Sr_2FeReO_6 consequently our efforts were put on the $Sr_2Fe_{1.33}Re_{0.67}O_6$ (x=0.33) monophasic sample (Fig. 1b). For such a composition, as shown in Table 1 and Fig. 1b, refinement of the structure in the *I*4/*m* SG leads to the formula $Sr_2(Fe_{0.87}Re_{0.13})_{2b}(Fe_{0.49}Re_{0.51})_{2a}O_6$ which can be written $Sr_2Fe_{1.36}Re_{0.64}O_6$, i.e. close to the nominal one.

Nominal (refined) x values	Refined crystallographic formula	a (Å) c (Å) V (Å³)	SG	χ^2	R_{Bragg}
0.0 (0.0)	$Sr_2(Fe)_{2b}(Re)_{2a}O_6$	5.5621(1) 7.8987(1) 244.360(5)	I4/m	4.46	5.12
0.25 (0.26)	$Sr_2(Fe_{0.91}Re_{0.09})_{2b}(Fe_{0.35}Re_{0.65})_{2a}O_6$	5.5639(1) 7.8820(2) 244.004(9)		2.19	7.01
0.33 (0.36)	$Sr_2(Fe_{0.87}Re_{0.13})_{2b}(Fe_{0.49}Re_{0.51})_{2a}O_6$	5.5628(1) 7.8739(2) 243.655(7)		4.09	4.52
0.37 (0.37)	$Sr_2(Fe_{0.85}Re_{0.15})_{2b}(Fe_{0.52}Re_{0.48})_{2a}O_6$	5.5684(2) 7.8701(6) 244.03(2)		2.30	7.38
0.50 (0.50)	$Sr_2(Fe_{0.72}Re_{0.28})_{2b}(Fe_{0.78}Re_{0.22})_{2a}O_6$	5.5693(1) 7.8853(2) 244.583(9)		2.97	7.65
0.75 (0.76)	$SrFe_{0.88}Re_{0.12}O_3$	3.90532(4) 59.562(1)	$Pm\bar{3}m$	3.41	4.19

Table 1: Cell parameters and formula from structure refinements using RT XRPD data (oxygen stoichiometry is set at 6).

This is also consistent with the one extracted from EDX analysis coupled to high resolution TEM (Fig. 1c). The corresponding image and superimposed model, calculated from crystallographic parameters, confirm that Re and Fe are not randomly distributed on the 2a and 2b crystallographic sites.
The magnetic susceptibility (χ) measurements show that χ at 5K decreases by a factor of 52 as x increases from 0.0 to 0.5 in $Sr_2Fe_{1+x}Re_{1-x}O_6$ (Fig. 2a) and that the T_C are above 400K. The rapid decrease of M_S with x increasing is illustrated by the $M(H)_{300K}$ curves of the x=0.00 and 0.33 compounds (inset of Fig. 2b). For $Sr_2Fe_{1.33}Re_{0.67}O_6$, the almost saturated M values in 5T are found to remain constant in between 5K and 300K (Fig. 2b), the coercive magnetic field H_C decreasing from 0.65T at 5K to ≈0.1T at 300K. This M_S=0.67μ_B/f.u. value can be compared to the one calculated from the formula. This can be done only if the Fe and Re oxidation states are known. The latter determined by electron energy-loss magnetic chiral dichroism were found to be Fe^{3+} and Re^{5+} for Sr_2FeReO_6 synthetized by using a Re excess [18-20]. The Fe K-edge XANES spectra of our three samples show similar features (Fig. 1d), pre-edge, absorption edge and white line positions are found at identical energies. Comparison with the iron references, Fe_2O_3 (Fe^{3+}) and FeO (Fe^{2+}), clearly shows that absorption edge coincides with that of Fe_2O_3 and thus that iron is trivalent in the three samples.

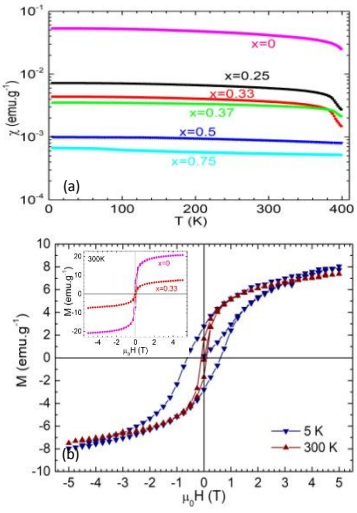

Figure 2: (a) χ(T) curves for the $Sr_2Fe_{1+x}Re_{1-x}O_6$ samples; x values (≤0.75) are labelled in the graph ($\mu_0H=10^{-2}$T, zfc process). (b) M(H) isothermal curves for $Sr_2Fe_{4/3}Re_{1/3}O_6$ at 5K and 300K. Inset: 300K M(H) curves for $Sr_2Fe_{1.33}Re_{0.67}O_6$ and Sr_2FeReO_6.

Along the series, Re^{5+} is supposed to change progressively to Re^{6+} (up to x=0.33) and then to Re^{7+} beyond 0.33, or the oxygen content does not remain six and oxygen vacancies appear in the lattice as x increases. From the x=0.0 result [20] and by taking the complete antiferromagnetic (AF) alignment of the Fe^{3+} (S=5/2) and Re^{5+} (S=1) magnetic moments in a 1Fe:1Re fully ordered double perovskite lattice, one expects $M_S=3\mu_B$/f.u.. Our x=0.0 sample shows a reduced magnetization value at 300K, i.e. $M_S=1.9\mu_B$/f.u., as already reported [14, 17], which is probably related to the difficulty in obtaining a monophasic sample with a perfect 1Fe:1Re order. Increasing x from x=0.0 in $Sr_2Fe_{1+x}Re_{1-x}O_6$ requires to increase the Fe and/or Re oxidation states. According to references [18-20], Re is oxidized into Re^{6+} in $Sr_2Fe_{1.2}Re_{0.8}O_6$ (x=0.2). The exchanges Fe^{3+}-O-Re^{5+}, Fe^{3+}-O-Re^{6+} (similar to the Fe^{3+}-O-Mo^{5+} AF double exchange in Sr_2FeMoO_6 [13]) and Fe^{3+}-O-Fe^{3+} are all AF. For x=0.33, as our XANES analysis points towards trivalent iron, it makes sense to have Re^{6+} in agreement with the "O_6" ideal oxygen stoichiometry, as both oxidation states are the most stable, in agreement with the easier synthesis for that composition compared to other x. This x=0.33 composition, ideally written as $Sr_2(Fe^{3+})_{2b}(Fe_{0.33}{}^{3+}Re_{0.67}{}^{6+})_{2a}O_6$, i.e. if fully ordered, yields $Ms=5\mu_B-[1.65\mu_B(Fe^{3+})+0.67\mu_B(Re^{6+})]= 2.68\mu_B$/f.u. which is much higher than the measured maximum value (Fig. 2b), $M_S=0.67\mu_B$/f.u. at 5K in 5T. This confirms the existence of Fe / Re anti-site defects as expressed by the formula coming from the structural refinement (Table 1). The existence of antiphase boundaries, created by anti-site defects aggregation, is proposed [20] to explain this low M_S in addition to the anti-site defects at play in the x=0.33 compound. A very different origin might also be invoked as the presence of the 5d cations characterized by strong spin orbit coupling with quenched orbital moment could severely reduce the effective magnetic moment as shown in iridates [23].

The rapid χ and M_S decrease with x can be related to the semiconducting-like electrical resistivity characterized by ρ_{300K} values increasing (Fig. 3) by a factor greater than 2000 from x=0.0 to 0.5. Nevertheless, our x=0.33 compound exhibits still negative magnetoresistance (MR) properties, reaching at 50K in 9T an effect of -11%, as compared to -16% for Sr_2FeReO_6 (Fig. 4). The butterfly shape of the MR(H) curves fits well with the M(H) curves at the same temperature with two MR maxima at H values corresponding to H_c in Fig. 2b. For the x=0.5 sample

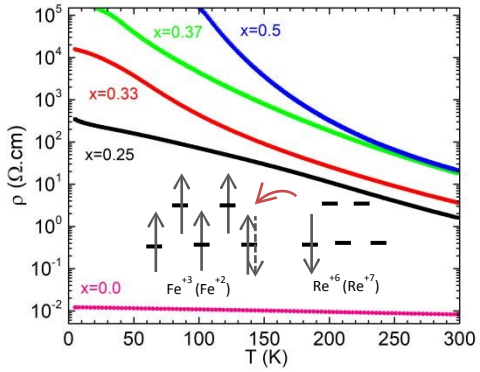

Figure 3: ρ(T) curves of $Sr_2Fe_{1+x}Re_{1-x}O_6$ samples. x values are labelled in the graph. Inset: schematic picture of the AF double-exchange mechanism.

(Fig. 4), the MR is almost completely suppressed. According to the Fe and Re distribution and assumed oxidation states, the MR disappearance, when going from x=0.33 to 0.5, could be explained by the fact that, for x > 0.33 oxygen vacancies appear or Re^{6+} becomes Re^{7+}, which in both cases suppresses the double exchange interaction. This is consistent with the charge delocalization mechanism in the ordered magnetic state as depicted in the inset of Fig. 3. When the Fe^{3+} magnetic moment is AF aligned to that of a neighbouring Re^{6+}, a double exchange mechanism allows the down spin of the Re^{6+} t_{2g} electron to be moved to the t_{2g} orbital of up spins of Fe^{3+} to create a Fe^{2+}. This Fe^{3+}+Re^{6+}↔Fe^{2+}+Re^{7+} double exchange mechanism explains the antiferromagnetic coupling and charge delocalization in the t_{2g} band.

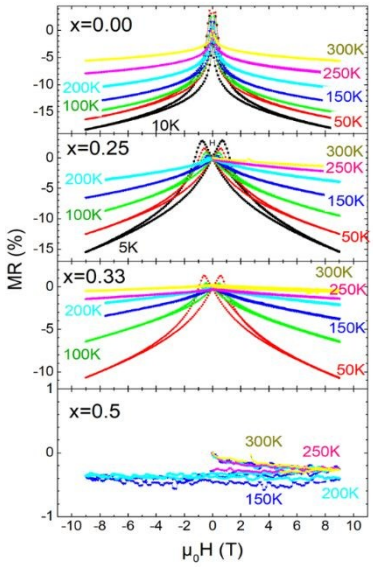

Figure 4: Isothermal magnetoresistance MR%=100x[(ρ(H)-ρ(H=0))/ρ(H=0)] curves of $Sr_2Fe_{1+x}Re_{1-x}O_6$ samples (x=0, 0.25, 0.33 and 0.5). T values are labelled in the graph.

This first dataset indicates that $Sr_2Fe_{1.33}Re_{0.67}O_6$ is a magneto-resistive ferrimagnet characterized by a T_C higher than RT. Considering the Fe^{3+} and Re^{6+} oxidation states in most cases of the series, the electronic transport properties are expected to be determined by the AF Fe^{3+}-O-Re^{6+} double-exchange, like Fe^{3+}-O-Mo^{5+} in Sr_2FeMoO_6. As a consequence of the Fe/Re = 2 ratio for x=0.33 and corresponding anti-site defects, numerous AF Fe^{3+}-O-Fe^{3+} super-exchange insulating regions exist and thus only the remaining AF Fe^{3+}-O-Re^{6+} double-exchange ones contribute to the charge delocalization mechanism. This explains at least partially the ρ increase with x in $Sr_2Fe_{1+x}Re_{1-x}O_6$. In that respect as S is dominated by the more conductive

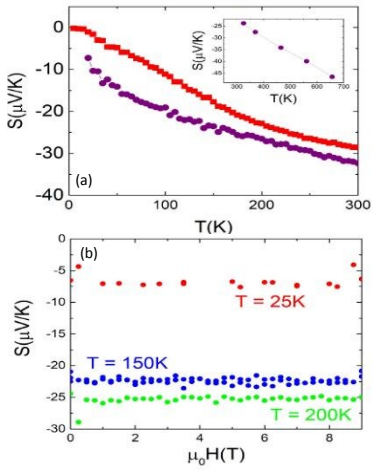

Figure 5: (a) S(T) curves for two samples $Sr_2Fe_{1.33}Re_{0.67}O_6$ between 5K and 300K. Inset : S(T) measured up to 660K. (b) Magnetothermopower curves S(H) measured for $Sr_2Fe_{1.33}Re_{0.67}O_6$ (corresponding to the purple symbols in Figure 6a).

pathways, the TEP measurements of $Sr_2Fe_{1.33}Re_{0.67}O_6$ give some clues about this scenario. The S(T) curves (Fig. 5a) measured for two samples are characterized by negative values with a linear slope on a broad temperature range supporting the existence of a metallic behaviour along the Fe^{3+}-O-Re^{6+} pathways. Interestingly, the value of S=-47μV.K^{-1} at 660K (inset of Fig. 5a) is not very different from S≈-30μV.K^{-1} in Sr_2FeMoO_6 at the same temperature [6]. The slope of the S(T) curve at high T enables a crude estimate of the carrier concentration, using a simple metallic Boltzmann model. Assuming an effective mass of $1m_e$ gives a carrier density close to $1.8{\cdot}10^{20}cm^{-3}$, which is close to the value ≈ $1.5{\cdot}10^{20}cm^{-3}$ in Sr_2FeMoO_6 [6], although the Fe/Re composition deviates from 1. The much larger resistivity of $Sr_2Fe_{1.33}Re_{0.67}O_6$ could thus come from the presence of antisite defects or microstructural effects.

A series of MTEP [S(H)] measurements of $Sr_2Fe_{1.33}Re_{0.67}O_6$ were performed from 5K to 300K (Fig. 5b), i.e. in its magnetically ordered state. They clearly reveal a lack of H effect on S for this temperature range. This result is interesting as it is a case of a magnetically ordered material which exhibits MR properties but without MTEP ones, different from what is typically observed in manganites such as $La_{0.95}Sr_{0.05}Mn_{0.95}Co_{0.05}O_3$ [9].

Conclusions

This study shows that $Sr_2Fe_{1.33}Re_{0.67}O_6$ (x=0.33) is an ordered double perovskite with degraded magnetic properties compared to Sr_2FeReO_6 (x=0.0 sample), resulting from the deviation from the ideal 1Fe:1Re composition. The existence of numerous anti-site defects and antiphase boundaries reported even for Sr_2FeReO_6 [18-20] hinders a perfect Fe↑Re↓ ferrimagnetic state setting, and the resulting magnetization is severely reduced. Such disordering obviously affects the transport properties as illustrated by the larger resistivity of $Sr_2Fe_{1.33}Re_{0.67}O_6$ as compared to Sr_2FeReO_6 associated with the decrease of the conducting pathways.

From that picture, the metallic behaviour can be understood by the TEP measurements, as this quantity probes the most conductive regions. As the S(H) measurements are performed in the ordered magnetic state (T≤300K), the AF coupling at the atomic scale of magnetic moments of adjacent Fe^{3+} and Re^{6+} cations leads to net spontaneous ferromagnetic component in the ferrimagnetic conducting domains. The Seebeck effect probes the electrons delocalized in these domains. As a result, upon magnetic field application, nothing being changed in the magnetism at the atomic level, i.e. local magnetic moments being already AF coupled, the TEP is unchanged. Finally, as compared to the other ferrimagnetic double perovskite Sr_2FeMoO_6 [6], in terms of thermoelectric performance, the higher electrical resistivity of $Sr_2Fe_{1+x}Re_{1-x}O_6$ is a detrimental factor. In that respect, only a strict control of the cationic order of this double perovskite would allow to optimize ρ.

Conflicts of interest

"There are no conflicts to declare".

C.M., A.M. and R.E.C. thank CNRS-CONICET 2014 (EDC26467), CONICET, PIP No. 11220120100360, the ANPCyT, PICT No. 2016–2495, and SECyT-UNC, Project No. 113/17 for financial support.

Notes and references

1 T. Okuda et al, Phys. Rev. B, 2001, **63**, 113104.
2 M. Mikami and K. Ozaki, J. Phys.: Conf. Ser., 2012, **379**, 012006.
3 E. Guilmeau et al, J. of Appl. Phys. 2009, **106**, 053715.
4 P. Jood et al, RSC Adv., 2014,**4**, 6363.
5 A. Maignan et al, Crystal Engineering, 2002, **5**, 365.
6 S. Popuri et al, Dalton Trans., 2015, **44**, 10621.
7 A.C. Masset et col., Phys. Rev. B, 2002, **62**, 166.
8 Y. Klein et al, Phys. Rev. B, 2006, **73**, 052412.
9 A. Kumar et al., Materials Research Express, 2018, **5**, 086110.
10 Y. Wang et al. Nature 2003, **423**, 425.
11 P. Limelette et al., Phys. Rev. Lett. 2006, **97**, 046601.
12 D. Berthebaud et al, J. Appl. Phys. 2018, **124**, 063905.
13 K. Kobayashi et al, Nature 1998, **395**, 677.
14 K. Kobayashi et al, Phys. Rev. B 1999, **59**, 11159.
15 E. V. Pannunzo Miner et al, Physica B 2007, **398**, 397.
16 N. Auth et al, J. Magn. Magn. Mater. 2004, **272-276**, e607.
17 M. Retuerto et al, Mater. Res. Bull. 2009, **44**, 1261.
18 S.Y. Choi et al, Microsc. Microanal. 2013,**19**, 25.
19 T.W. Lim et al, Sci. Rep. 2016, **6**, 19746.
20 P.L. Ho et al, Ultramicroscopy 2018, **193**, 137.
21 J. Rodríguez-Carvajal, Physica B,1993, **192,** 55.
22 B. Ravel and M. Newville, J. of Synchrotron Radiation 2005, **12**, 537.
23 B. J. Kim et al., Phys. Rev. Lett. 101, 076402 (2008).